Optimization of the CMB-galaxy cross-correlation signal for studying the Integrated Sachs-Wolfe effect

Arthur Diniz Meirelles

Advisor: Edivaldo Moura Santos
Coadvisor: Ronaldo Carloto Batista

Institute of Physics
Universidade de São Paulo

15/08/2024

Introduction

- The integrated Sachs-Wolfe (ISW) effect occurs due to time changes in gravitational potentials;
- During periods of transition from or to matter-dominated eras of the Universe, potentials change more rapidly;
- Naturally, a statistical correlation between CMB temperature maps and gravitational potentials is expected.

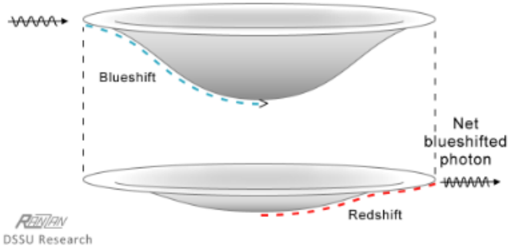

Figure 2: Illustration of the ISW effect. In this case, the gravity wells flattened, leaving a net blueshift.

The ΛCDM Model

To build the theoretical framework used, it is assumed

- The Universe is homogeneous and isotropic at large scales;
- Initial conditions are obtained by assuming an inflationary period when the Universe was very compact and energetic;
- The Universe is composed of baryonic matter, radiation, neutrinos, cold dark matter and a dark energy component described by a cosmological constant Λ;

The homogeneous and isotropic background is first set up, and linear perturbations are added to it.

The Perturbed Metric

We express the perturbed Friedman-Lemaître-Robertson-Walker (FLRW) metric with two functions $\Psi(\mathbf{x}, t)$ and $\Phi(\mathbf{x}, t)$

$$\begin{cases} g_{00} = -1 - 2\Psi(\mathbf{x}, t), \\ g_{0i} = g_{i0} = 0, \\ g_{ij} = a^2(t)\delta_{ij}[1 + 2\Phi(\mathbf{x}, t)]. \end{cases} \tag{1}$$

The ΛCDM Model

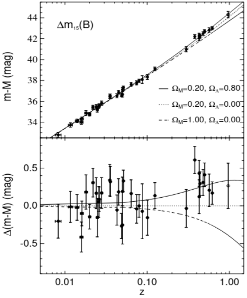

Figure 3: Distance modulus comparing different cosmological constants. Extracted from Adam G. Riess et al. “Observational Evidence from Supernovae for an Accelerating Universe and a Cosmological Constant” (1996).

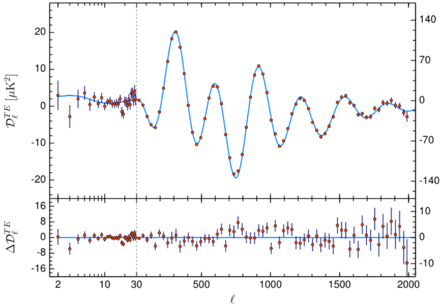

Figure 4: CMB temperature and polarization cross-correlation spectrum. Extracted from Planck Collaboration et al. "Planck 2018 results. VI. Cosmological Parameters" (2018).

The Cosmic Microwave Background

The temperature of the Cosmic Microwave Background (CMB) can be expressed by

$$T(\mathbf{x}, \hat{\mathbf{p}}, t) = \bar{T}(t)\left[1 + \Theta(\mathbf{x}, \hat{\mathbf{p}}, t)\right]. \tag{2}$$

The temperature perturbation Θ can be expressed in Fourier space according to

$$\Theta(\hat{\mathbf{k}}, \mu) = \sum_{\ell=0}^{\infty} (2\ell + 1)(-i)^{\ell}\Theta_{\ell}(\hat{\mathbf{k}})\mathscr{P}_{\ell}(\mu), \tag{3}$$

where $\mu = \hat{\mathbf{k}} \cdot \hat{\mathbf{p}}$ and $\mathscr{P}_{\ell}$ are Legendre polynomials.

Analytical Approximation

Working with first-order equations and the tightly coupled limit, and assuming recombination to be an instantaneous process happening at conformal time $\eta = \eta*$, we can obtain

$$\begin{aligned}\Theta_\ell(k,\eta_0) \approx & [\Theta_0(k,\eta_*) + \Psi(k,\eta_*)] j_\ell[k(\eta_0-\eta_*)] \\ & + i v_b(k,\eta_*) \left\{ j_\ell[k(\eta_0-\eta_*)] - (\ell+1)\frac{j_\ell[k(\eta_0-\eta_*)]}{k(\eta_0-\eta_*)} \right\} \\ & + \int_0^{\eta_0} d\eta e^{-\tau} [\Psi'(k,\eta) - \Phi'(k,\eta)] j_\ell[k(\eta_0-\eta)].\end{aligned} \tag{4}$$

Here, the third term in the equation describes the Integrated Sachs-Wolfe effect.

Correlation Functions

To calculate the CMB autocorrelation function C_ℓ^{tt}, we expand Θ in spherical harmonics

$$\Theta(\mathbf{x}, \hat{\mathbf{p}}, t) = \sum_{\ell=1}^{\ell_{\max}} \sum_{m=-\ell}^{\ell} a_{\ell m}(\mathbf{x}, t) Y_{\ell m}(\hat{\mathbf{p}}), \tag{5}$$

and calculate the autocorrelation between the $a_{\ell m}$ terms:

$$\langle a_{\ell m} a^*_{\ell' m'} \rangle = \delta_{\ell \ell'} \delta_{m m'} C_\ell^{tt} \tag{6}$$

Other autocorrelation spectra C_ℓ^{xx} follow the same process. It is common to use $D_\ell^{XX} = \frac{\ell(\ell+1)}{2\pi} C_\ell^{xx}$ for some spectra for better visualization. We can also write

$$C_\ell^{tt} = \frac{1}{2\ell+1} \sum_{m=-\ell}^{\ell} a_{\ell m} a^*_{\ell' m'} \tag{7}$$

Cosmic Variance

The low number of $a_{\ell m}$ coefficients for lower multipoles ℓ leads to a high uncertainty in this region called cosmic variance

$$\left(\frac{\Delta C_\ell^{XX}}{C_\ell^{XX}}\right)_{CV} = \sqrt{\frac{2}{2\ell + 1}} \tag{8}$$

Planck 2018

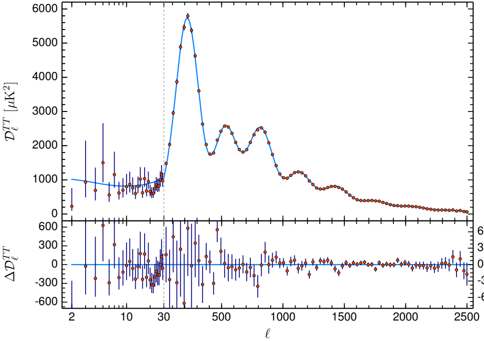

Figure 5: Planck 2018 CMB temperature power spectrum. Figure and table extracted from Planck Collaboration et al. "Planck 2018 results. VI. Cosmological Parameters" (2018).

Parameter	Best-fit
$\Omega_b h^2$	0.02237 ± 0.00015
$\Omega_c h^2$	0.1200 ± 0.0012
$100\Theta_{MC}$	1.04092 ± 0.00031
τ	0.0544 ± 0.0073
$\ln(10^{10} A_s)$	3.044 ± 0.014
n_s	0.9649 ± 0.042
Ω_m	0.3153 ± 0.0073
H_0	67.36 ± 0.54 km/s/Mpc
σ_8	0.8111 ± 0.0060

Table 1: Best-fit values of cosmological parameters using TT+TE+EE+lowE and gravitational lensing data.

CMB Autocorrelation Contributions

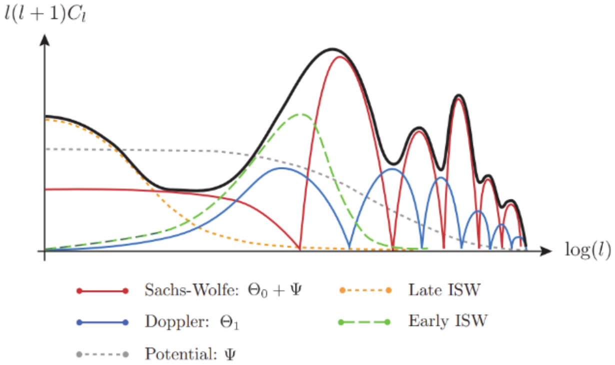

Figure 6: Contributions to the CMB autocorrelation power spectrum. Extracted from D. Baumann, "Lecture notes in Advanced Cosmology" (2014).

The Matter Power Spectrum

To calculate a cross-correlation function, we need the 3D matter power spectrum $P(k, z)$, defined by

$$\left\langle \delta(\mathbf{k}, z)\delta^*(\mathbf{k}', z) \right\rangle = (2\pi)^3 P(k, z)\delta_D(\mathbf{k}-\mathbf{k}')$$

We have used CAMB's implementation of the HALOFIT model to calculate the matter power spectrum.

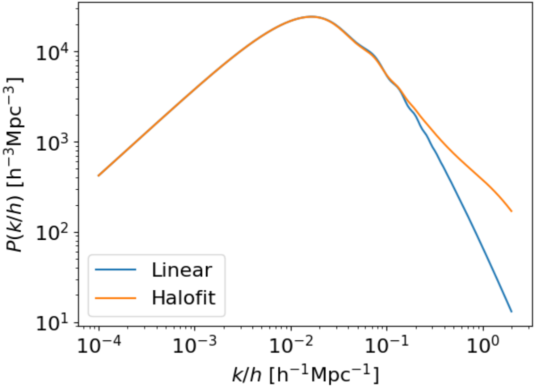

Figure 7: Matter power spectrum calculated using both a linear approximation and the HALOFIT model.

The Cross-correlation Spectrum

To trace the matter density anisotropies, we used galaxy contrast maps, which can be calculated using

$$\delta_g(\mathbf{n}) = \frac{N_g(\mathbf{n}) - \bar{N}_g}{\bar{N}_g} \tag{9}$$

It is assumed that $\delta_g = b_g \delta$, where b_g is the bias factor, which we assume to be a slowly varying function of redshift.

The galaxy autocorrelation C_ℓ^{gg} and cross-correlation function C_ℓ^{tg} can then be calculated with

$$\langle a^t_{\ell m} a^g_{\ell' m'} \rangle = C_\ell^{tg} \delta_{\ell \ell'} \delta_{mm'} \qquad \langle a^g_{\ell m} a^g_{\ell' m'} \rangle = C_\ell^{gg} \delta_{\ell \ell'} \delta_{mm'} \tag{10}$$

Analytical Formula

Given fields x and y, representing either the ISW contribution to the CMB temperature $(x, y = t)$ or the galaxy contrast $(x, y = g)$, we can calculate the associated auto- or cross-correlation spectra using

$$C_\ell^{xy} = \frac{2}{\pi} \int dk k^2 W_\ell^x(k) W_\ell^y(k) P(k), \tag{11}$$

with

$$W_\ell^t = -3\Omega_m \left(\frac{H_0}{k}\right)^2 \int dz \frac{\mathrm{d}[(1+z)D(z)]}{\mathrm{d}z} j_\ell[k\chi(z)] \tag{12}$$

$$W_\ell^g = \int dz b_g(z) \frac{\mathrm{d}N}{\mathrm{d}z} D(z) j_\ell[k\chi(z)] \tag{13}$$

ISW Contribution: Temperature Autocorrelation

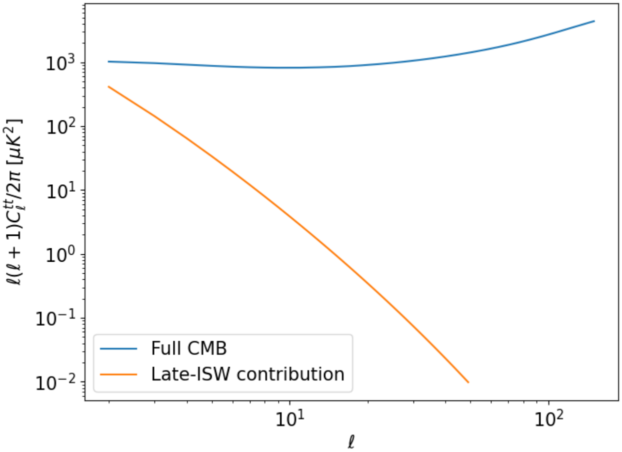

Figure 8: CMB autocorrelation comparison between full spectrum and ISW contribution.

ISW Contribution: Galaxy Autocorrelation and Cross-correlation

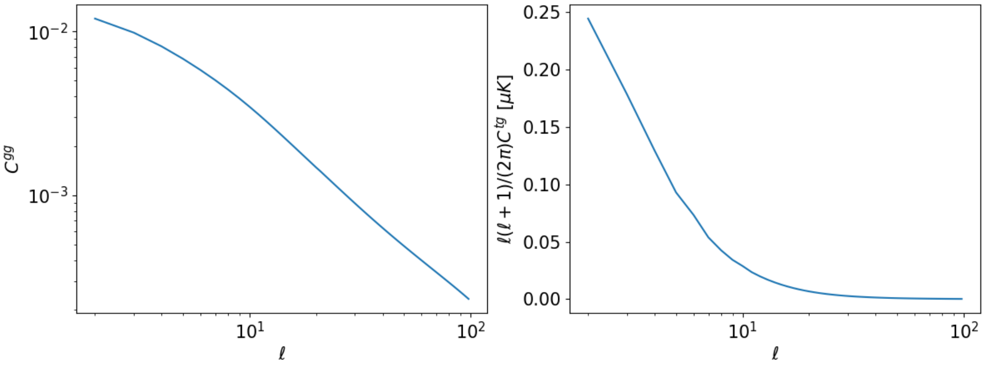

Figure 9: Galaxy autocorrelation spectrum (left) and late-ISW contribution to the galaxy-CMB cross-correlation (right).

Selection Function Parametrization

The function $\frac{\mathrm{d}N}{\mathrm{d}z}$ in equation (13) is called the selection function. We are assuming its parametrization to be[1].

$$\frac{\mathrm{d}N}{\mathrm{d}z}(z|\lambda,\beta,z_0)\,dz = \frac{\beta}{\Gamma(\lambda)}\left(\frac{z}{z_0}\right)^{\beta\lambda-1}\exp\left[-\left(\frac{z}{z_0}\right)^{\beta}\right]d\left(\frac{z}{z_0}\right) \tag{14}$$

We have explored how to maximize the cross-correlation signal using an idealized selection function.

[1] Afshordi et al. "Cross-correlation of the cosmic microwave background with the 2MASS galaxy survey: Signatures of dark energy, hot gas, and point sources" (2004).

2MASS Bands Comparison

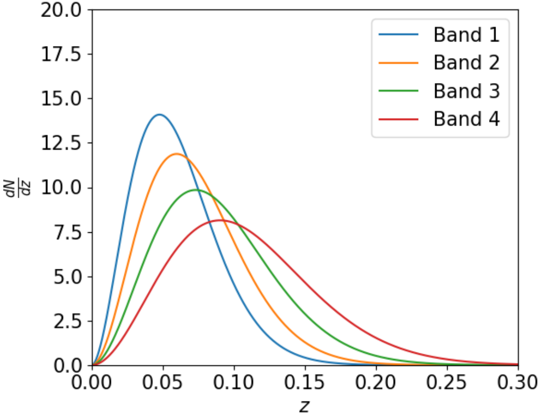

Figure 10: Selection function calculated for the 4 bands of the 2MASS catalog.

Band	z_0	β	λ
1	0.043	1.825	1.524
2	0.054	1.800	1.600
3	0.067	1.765	1.636
4	0.084	1.723	1.684

Table 2: Parameter values for the 4 bands of the 2MASS catalog.

Exploring the Parameter Space

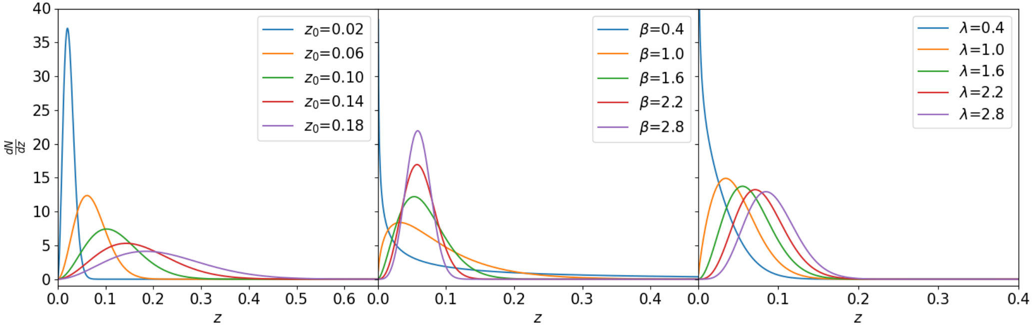

Figure 11: Selection function calculated for various parameter values.

Null Hypothesis

For the process of finding a galaxy survey with an idealized selection function, we first needed an estimation for the probability of C_ℓ^{tg} being 0, which would be our null hypothesis. The following process was used:

- Synthesize multiple uncorrelated CMB temperature and galaxy contrast maps using HEALPix;
- Calculate the cross-correlation C_ℓ^{tg} for each pair of uncorrelated maps at each multipole;
- For each multipole ℓ, a histogram of C_ℓ^{tg} was produced;
- Each histogram was fit with Gaussian distributions with average $\mu = \mu_\ell \approx 0$ and $\sigma^2 = \sigma_\ell^2$.

The null hypothesis is compatible with $\Omega_m = 1$.

Synthesized Maps' Null Hypothesis Histograms

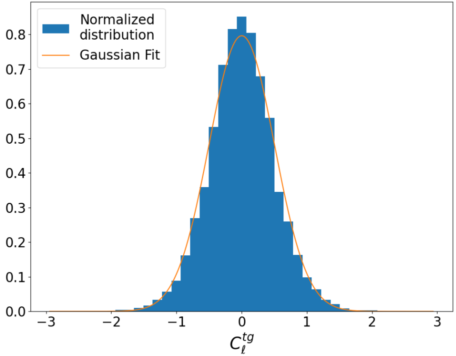

(a) $\ell = 4$

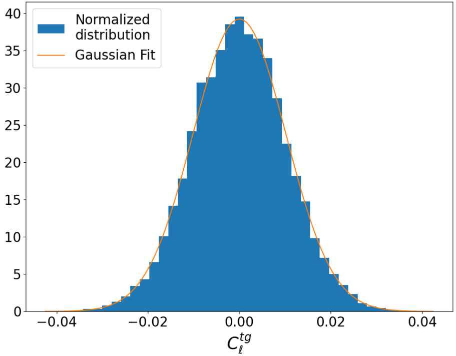

(b) $\ell = 30$

Figure 12: Distribution of cross-correlation values on different multipoles for 10^4 maps synthesized with null cross-correlation.

Null Hypothesis

For f_ℓ corresponding to the Gaussian fit made for the multipole ℓ

$$f_\ell(C_\ell^{tg}) = \frac{1}{\sqrt{2\pi\sigma_\ell^2}} \exp\left[-\frac{1}{2}\left(\frac{C_\ell^{tg} - \mu_\ell}{\sigma_\ell}\right)^2\right], \tag{15}$$

we have defined the null hypothesis probability distribution to be

$$P_{\text{null}} = \prod_{\ell=2}^{\ell_{\text{max}}} f_\ell(C_\ell^{tg}) \tag{16}$$

Exploring the Parameter Space

For various points (β, z_0, λ) in the parameter space, we have calculated the ratio $P_{\text{null}}(\beta, z_0, \lambda)\,/\,P_{\text{null}}^{\text{2MASS}}$ and produced the heat maps in Figure 13.

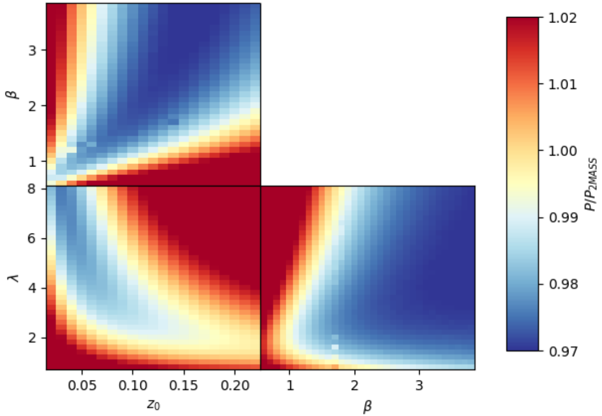

Figure 13: Heat maps used to explore the parameter space.

Minimizer

The heat maps provided initial points to run an algorithm that minimizes $P_{\text{null}}(z_0, \beta, \lambda)$. The point found that minimizes the null hypothesis probability in that region of the parameter space was

$$(\beta, z_0, \lambda) = (3.088, 0.1508, 4.9401) \tag{17}$$

Properties of the Minimum

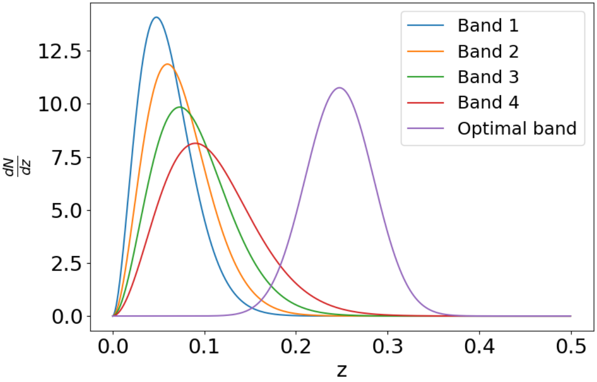

Figure 14: Selection functions comparison.

The selection function found is deeper than that of 2MASS band 1. It does not favor galaxies at $z^* = 0.63$, the estimated redshift at which the accelerated expansion started.

Properties of the Minimum

The selection function found reduces the maximum value of the cross-correlation function, but its peak is at higher redshifts ($\ell \approx 10$), reducing the influence of cosmic variance in the signal.

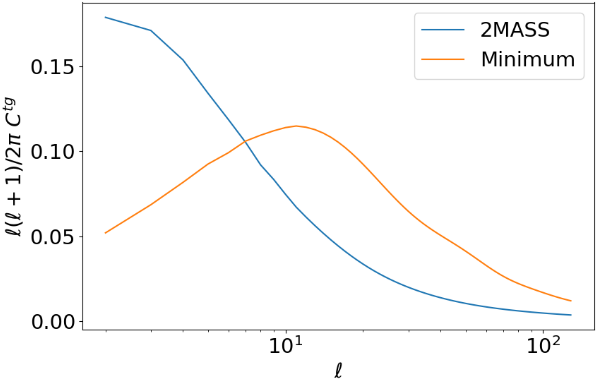

Figure 15: Theoretical cross-correlation spectrum comparison.

Discussion

- The ratio $P_{\text{null}}(z_0, \beta, \lambda) / P_{\text{null}}^{\text{2MASS}} = 0.971$ for the minimum;
- Despite the small statistical gain, this optimal selection function yields reasonably better results for constraints on Ω_m, as will be discussed;
- A similar work has reported a small preference towards the non-null signal with changes to the depth of the survey and fainter magnitude limits [1].

WMAP Data

The CMB temperature maps used in this project are the ones provided by WMAP9.

- Three frequency bands were used, which are named bands Q (40GHz), V (60GHz) and W (90GHz);
- The temperature intensity maps' noise power can be well modeled as uncorrelated Gaussian fluctuations;
- Despite having a lower resolution (0.3°) compared to Planck's (0.083°), this project focuses on lower multipoles;
- We have combined both maps' masks and used it for analysing each one, resulting in a fraction $f_{\text{sky}} = 0.7$.

WMAP Data

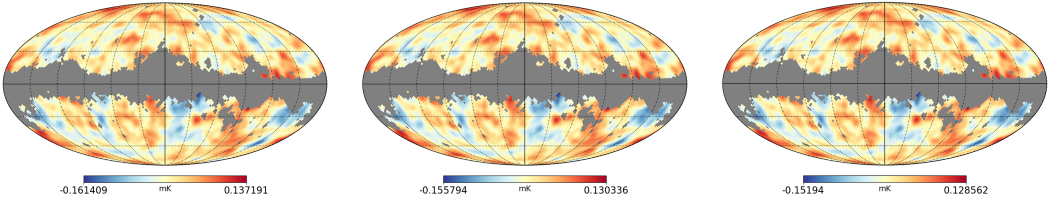

(a) Q channel (b) V channel (c) W channel

Figure 16: Mollweide projection of three (Q, V, W) WMAP9 CMB temperature (in mK) maps in galactic coordinates with an $f_{\rm sky} = 0.70$ mask applied

2MASS Catalog

Wide sky coverage is a very influential aspect of studying cross-correlation spectra, and the 2MASS catalog contains raw imaging data covering 99.998% of the sky, which was the dataset used.

- We have used the K_s (2.16 μm) band of the Extended Source Catalog (XSC);
- The data of the K_s band obtained from a 20 mag aperture (K_{20}) were corrected for galactic extinction, and the remaining data was further divided into 4 bands: Bands 1 ($12.0 < K'_{20} < 12.5$), 2 ($12.5 < K'_{20} < 13.0$), 3 ($13.0 < K'_{20} < 13.5$) and 4 ($13.5 < K'_{20} < 14.0$);
- Each band has a different selection function, as shown in Figure 10.

2MASS Catalog

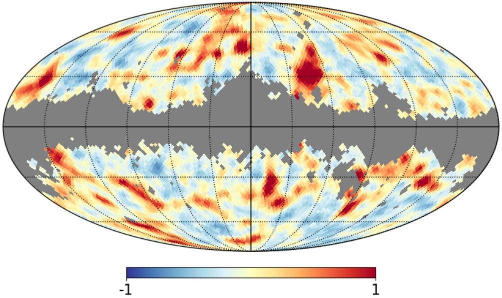

(a) Band 1

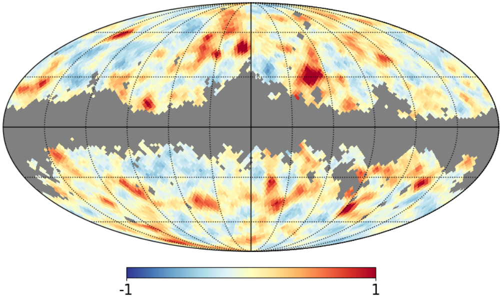

(b) Band 2

Figure 17: Mollweide projection of the 2MASS-XSC galaxy contrast maps in galactic coordinates with the combined 2MASS+WMAP mask applied ($f_{sky} = 0.70$).

2MASS Catalog

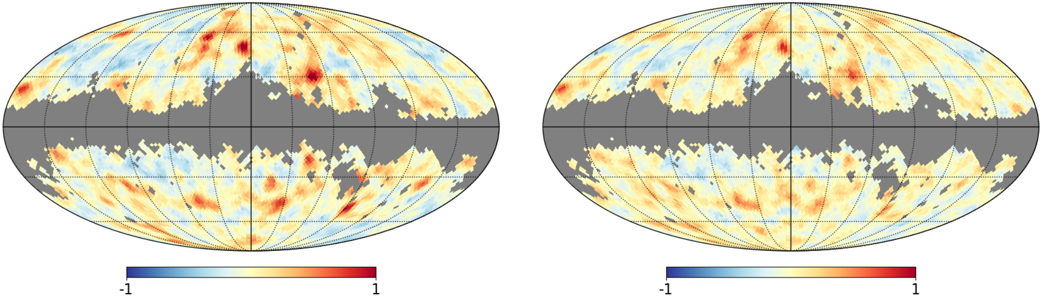

(a) Band 3 (b) Band 4

Figure 18: Mollweide projection of the 2MASS-XSC galaxy contrast maps in galactic coordinates with the combined 2MASS+WMAP mask applied ($f_{sky} = 0.70$).

Correlation Spectra Estimator

To estimate the correlation spectra that describe the pixelized maps d with primordial signal s and noise n (with $\mathbf{S}$ and $\mathbf{N}$ being the corresponding covariance matrices), we could use the following likelihood function.

$$\mathscr{L} = P(\mathbf{d}|\mathbf{C}) = \frac{1}{(2\pi)^{n_{\text{dim}}/2}|\mathbf{C}|^{1/2}} \exp\left(-\frac{1}{2}\mathbf{d}^T\mathbf{C}^{-1}\mathbf{d}\right), \qquad \mathbf{C} = \mathbf{S} + \mathbf{N} \tag{18}$$

With a prior $\pi(\mathbf{S})$ we can use Bayes' Theorem to obtain

$$P(\mathbf{C}|\mathbf{d}) \propto \pi(\mathbf{S}) P(\mathbf{d}|\mathbf{C}) \tag{19}$$

Correlation Spectra Estimator

If we can sample from $P(\mathbf{C}|\mathbf{s}, d)$ and $P(\mathbf{s}|\mathbf{C}, d)$. Then we iterate

$$\mathbf{s}^{i+1} \leftarrow P(\mathbf{s}|\mathbf{C}^{i}, d) \tag{20}$$

$$\mathbf{C}^{i+1} \leftarrow P(\mathbf{C}|\mathbf{s}^{i+1}, d), \tag{21}$$

to obtain a sample of $\{(\mathbf{s}^i, \mathbf{C}^i)\}$.

The Blackwell-Rao Estimator

We can then use the Blackwell-Rao estimator to obtain an approximation for $P(C_\ell|\mathbf{d})$

$$P(C_\ell|\mathbf{d}) \approx \frac{1}{N_G}\sum_{i=1}^{N_G} P(C_\ell|\sigma_\ell^i), \tag{22}$$

where

$$\sigma_\ell^i = \frac{1}{2\ell+1}\sum_{m=-\ell}^{\ell} \mathbf{s}_{\ell m}\mathbf{s}_{\ell m}^\dagger. \tag{23}$$

We then maximize the probability $P(C_\ell|\mathbf{d})$ to obtain the best-fit C_ℓ.

Matrices Used

In this work, **s** and **S** are defined by

$$\mathbf{s}^T = (s_{00}^{tg}, s_{01}^{tg}, s_{11}^{tg}, \ldots, s_{\ell_{\max}0}^{tg}, \ldots, s_{\ell_{\max}\ell_{\max}}^{tg}), \tag{24}$$

$$\mathbf{S} = \mathrm{diag}(S_0^{tg}, S_1^{tg}, S_1^{tg}, \ldots, S_{\ell_{\max}}^{tg}, \ldots, S_{\ell_{\max}}^{tg}), \tag{25}$$

where

$$\mathbf{s}_{\ell m}^{tg} = \begin{pmatrix} a_{\ell m}^{t} \\ a_{\ell m}^{g} \end{pmatrix}, \qquad \mathbf{S}_{\ell}^{tg} = \begin{pmatrix} C_\ell^{tt} & C_\ell^{tg} \\ C_\ell^{tg} & C_\ell^{gg} \end{pmatrix}. \tag{26}$$

Correlation Spectra Obtained

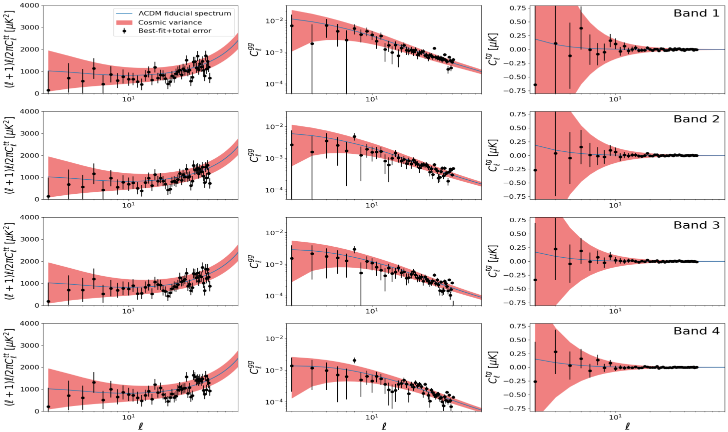

Figure 19: Comparison between theoretical correlation spectra and the ones estimated from WMAP and 2MASS.

Monte Carlo Markov Chains

By defining the likelihood $\mathscr{L}(C_\ell|\theta)$ and the prior $p(\theta)$, one can use Markov chains to obtain samples of each parameter in θ following the posterior

$$P(\theta|C_\ell) = \mathscr{L}(C_\ell|\theta)\,p(\theta) \tag{27}$$

Joint posteriors can be easily obtained from each parameter sample, strongly simplifying data analysis for multiple parameter models.

Planck Likelihoods

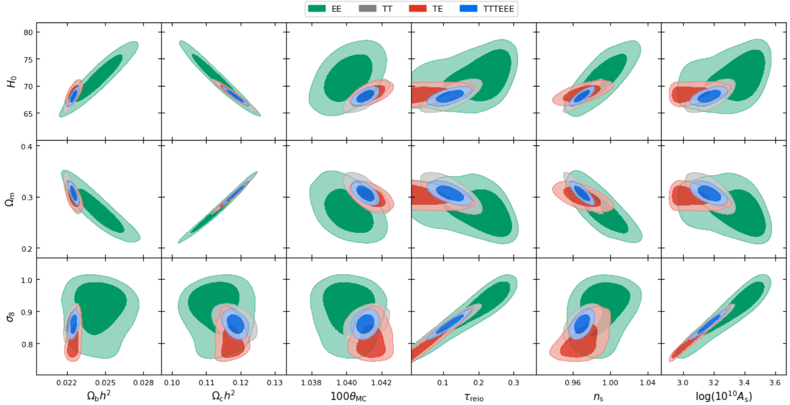

Figure 20: Joint posterior distributions of cosmological parameters using Planck's CMB temperature (T) and polarization (E) data.

Likelihood Profiling

The likelihood of each point in the spectrum was assumed to be Gaussian

$$\mathscr{L}(C^{xy}_{\ell,\,\text{theo}}|C^{xy}_{\ell,\,\text{data}}) = \frac{1}{\sigma_\ell\sqrt{2\pi}}\exp\left[-\frac{1}{2}\left(\frac{C^{xy}_{\ell,\,\text{data}} - C^{xy}_{\ell,\,\text{theo}}}{\sigma_\ell}\right)^2\right]. \tag{28}$$

We are varying only Ω_m, so $C^{xy}_{\ell,\,\text{theo}}$ is a functions of only Ω_m. The likelihood of a full spectrum is

$$\mathscr{L}(\Omega_m|C^{xy}_{\text{data}}) = \prod_{\ell=2}^{\ell_{\max}} \mathscr{L}(C^{\text{xy}}_{\ell,\,\text{theo}}|C^{\text{xy}}_{\ell,\,\text{data}}). \tag{29}$$

The $C^{tg} + C^{gg}$ joint-likelihood is

$$\mathscr{L}(\Omega_m|C^{tg}_{\text{data}}, C^{gg}_{\text{data}}) = \mathscr{L}(\Omega_m|C^{tg}_{\text{data}})\mathscr{L}(\Omega_m|C^{gg}_{\text{data}}). \tag{30}$$

Results for 2MASS

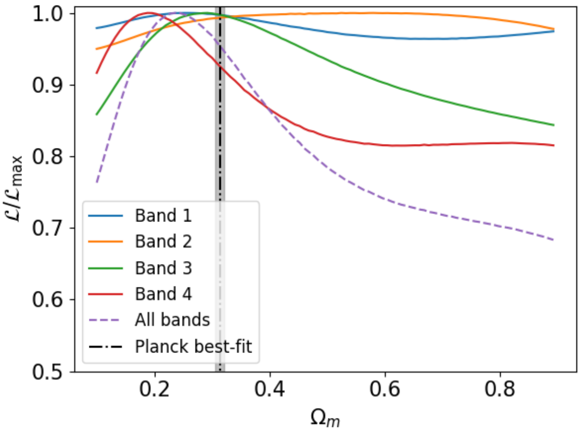

Figure 21: C^{tg} only likelihood profiles.

- All curves are compatible with Planck;
- Not much constraining power on Ω_m;
- Bands 3 and 4 – which have the deepest selection functions – have the most constraining power amongst all 4.

Results for 2MASS

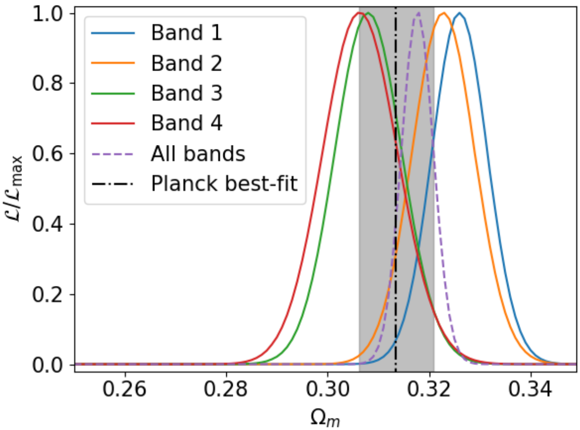

Figure 22: Joint likelihood profiles

- All likelihoods are compatible with Planck;
- Very high constraining power on Ω_m when C^{gg} is introduced, comparable to Planck's;
- No significant difference in constraining power between each band.

Forecast for the Optimized Band

To estimate the behavior of a survey that follows our idealized selection function in this analysis, we have produced two synthetic cross-correlation spectra using that selection function. Both use the ΛCDM model with Planck's best-fit parameters, only differing in Ω_m:

- One of the datasets was produced using Plancks best-fit of $\Omega_m = 0.3153$;
- The other dataset was produced using $\Omega_m = 0.188$, the value that maximizes the likelihood of band 4 for the C^{tg} only likelihood.

Band 4's errors were used as estimated for both synthetic datasets.

Forecast for the Optimized Band

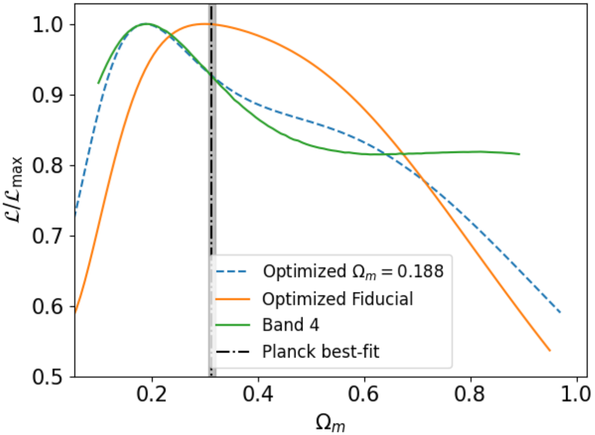

Figure 23: Optimized band C^{tg} only profile.

- Constraining power still low;
- Reasonable improvement in the constraining power.

Discussion

- The optimized band being deeper than 2MASS means errors on the spectra should be lower, meaning the errors used are overestimated, which indicates the constraints could be better for a real survey following our optimized selection function;
- The optimized band was not found by optimizing the Ω_m constraints, but rejecting the null cross-correlation hypothesis. $\Omega_m = 1$ leads to $C_\ell^{tg} = 0$, and the fast decrease in likelihood for higher Ω_m is noticeable.

1. Theoretical Aspects
2. Optimized Galaxy Survey
3. Data Processing
4. Analysis and Results
5. Conclusions

Conclusions

- We have obtained the likelihood profiles for Ω_m obtained from cross-correlation data by studying the ISW effect;
- The constraints obtained using only C^{tg} were not strong, but can be used as a complement to other datasets for a combined analysis;
- In the 2MASS catalog, the 2 deepest bands – bands 3 and 4 – yielded better constraining power;
- The Planck collaboration also studied the ISW effect using the cross-correlation spectrum[2], obtaining significantly better results with deeper surveys (NVSS and Planck's Kappa map).

[2] Planck Collaboration et al. "Planck 2015 results - XXI. The integrated Sachs-Wolfe effect" (2016).

Conclusions

- An optimized band capable of maximizing the ISW signal was obtained, prioritizing galaxies at higher redshifts and increasing the cross-correlation signal in a region less affected by cosmic variance;
- The likelihoods obtained for artificial data calculated using the optimized band improved the constraints on Ω_m;
- Combining different matter tracers leads to improved results overall.

Thank You

Blackwell-Rao Best-fit Solution

The best-fit solution for the posterior obtained using the Blackwell-Rao estimator is

$$\mathbf{S}_\ell = \frac{1}{2\ell + 1 + 2q}\bar{\sigma}_\ell \tag{31}$$

with

$$\bar{\sigma}_\ell = \frac{1}{N_G}\sum_{i=1}^{N_G}\sigma_\ell \tag{32}$$

Future Prospects

Exploring the growth function parametrization

$$\frac{\mathrm{d}\ln D(a)}{\mathrm{d}\ln a} = \Omega_m^\gamma(a), \qquad (33)$$

with γ as a free parameter might be worth to explore.

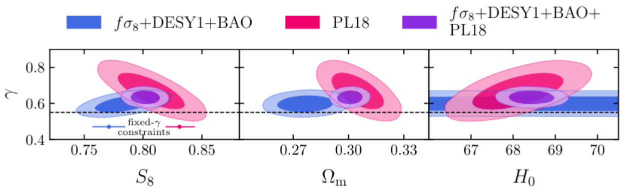

Figure 24: Figure extracted from Nhat-Minh Nguyen, Dragan Huterer, and Yuewei Wen. "Evidence for Suppression of Structure Growth in the Concordance Cosmological Model" (2023).

Bias Factor Fit

The bias factor was fitted to the data using the galaxy autocorrelation function with limiting multipoles for the linear model and HALOFIT.

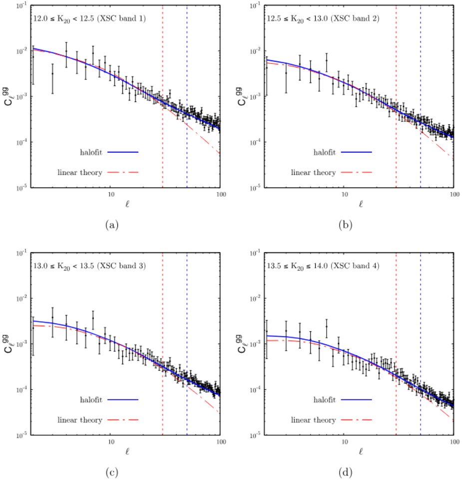

Bias Factor Fit

		Linear ($\ell_{max} = 30$)		Halofit ($\ell_{max} = 50$)		Halofit ($\ell_{max} = 96$)	
Band	Shot Noise	$b_g \pm \sigma_b$	χ^2/n dof	$b_g \pm \sigma_b$	χ^2/n dof	$b_g \pm \sigma_b$	χ^2/n dof
1	1.8×10^{-4}	1.27 ± 0.04	$19.1/28$	1.32 ± 0.02	$33.5/48$	1.37 ± 0.01	$127.3/94$
2	8.5×10^{-5}	1.25 ± 0.03	$17.3/28$	1.34 ± 0.03	$29.2/48$	1.35 ± 0.01	$102.1/94$
3	4.0×10^{-5}	1.22 ± 0.03	$16.9/28$	1.29 ± 0.02	$37.3/48$	1.34 ± 0.01	$86.2/94$
4	1.9×10^{-5}	1.18 ± 0.03	$32.2/28$	1.28 ± 0.02	$52.5/48$	1.29 ± 0.01	$105.9/94$

Figure and table extracted from E. Moura-Santos et al. “A Bayesian Estimate of the CMB–large-scale Structure Cross-correlation” (2016).

Planck Selection Functions

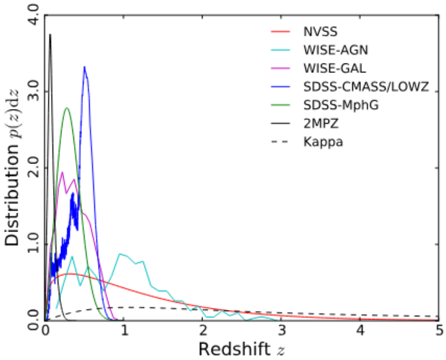

Figure 25: Selection functions of tracers used for Planck's analysis. Extracted from Planck Collabortaion et al. "Planck 2015 results. XXI. The integrated Sachs-Wolfe effect" (2016).

Influence of Parameters on C_ℓ^{tt}

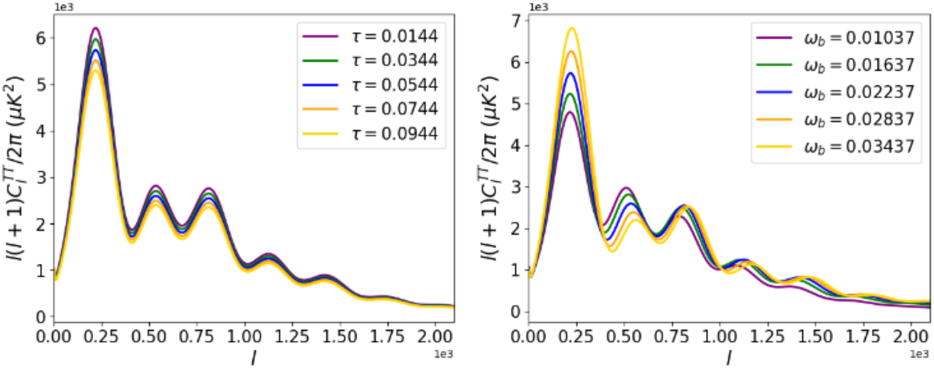

Figure 26: Extracted from Alexandra T. Petreca "The impact of systematic effects on the cosmic distance ladder" (2024)

Influence of Parameters on C_ℓ^{tt}

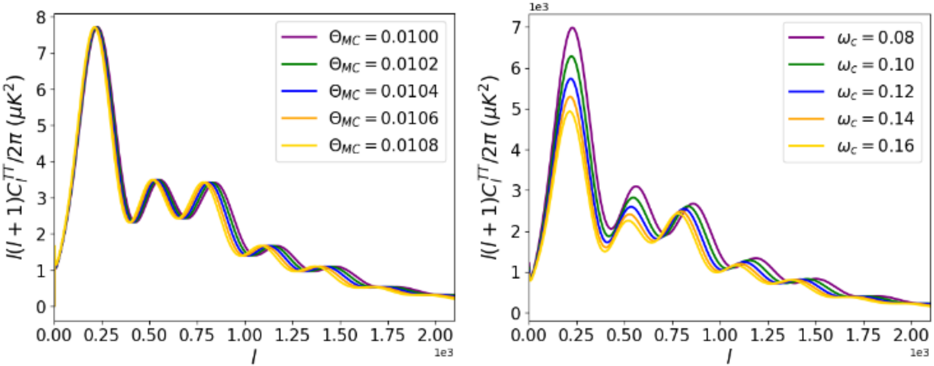

Figure 27: Extracted from Alexandra T. Petreca "The impact of systematic effects on the cosmic distance ladder" (2024)

Influence of Parameters on C_ℓ^{tt}

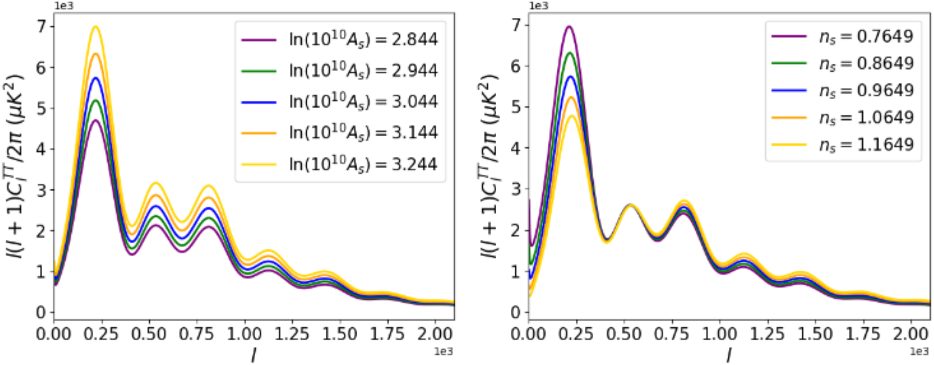

Figure 28: Extracted from Alexandra T. Petreca "The impact of systematic effects on the cosmic distance ladder" (2024)

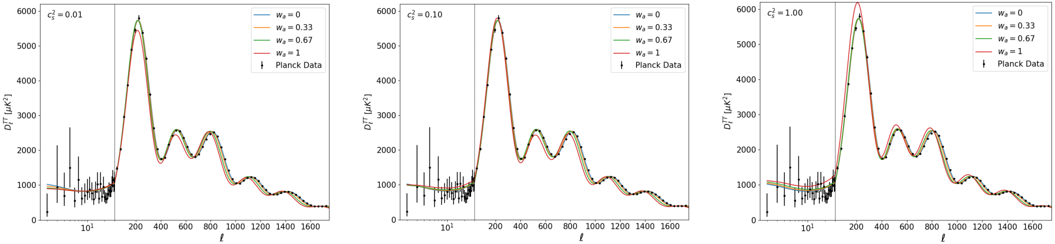

Figure 29: CPL parameters' influence on CMB temperature autocorrelation spectrum.

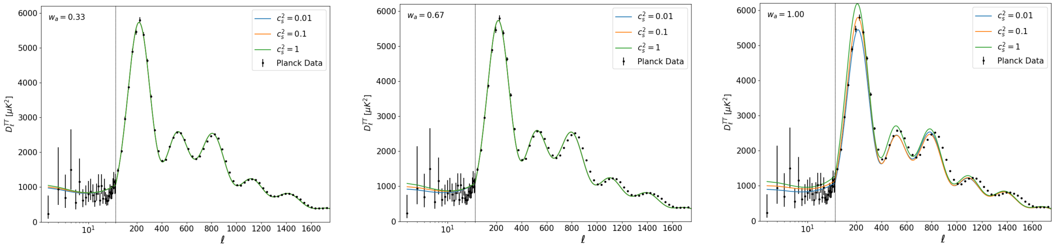

Figure 30: CPL parameters' influence on CMB temperature autocorrelation spectrum.